Available online at www.sciencedirect.com
ScienceDirect
Journal of Computational Physics 225 (2007) 591–614
JOURNAL OF COMPUTATIONAL PHYSICS
www.elsevier.com/locate/jcp

# A field-space-based level set method for computing multi-valued solutions to 1D Euler–Poisson equations

Hailiang Liu *, Zhongming Wang

*Iowa State University, Department of Mathematics, Ames, IA 50011, United States*

Received 15 May 2006; received in revised form 10 October 2006; accepted 18 December 2006
Available online 10 January 2007

**Abstract**

We present a field-space-based level set method for computing multi-valued solutions to one-dimensional Euler–Poisson equations. The system of these equations has many applications, and in particular arises in semiclassical approximations of the Schrödinger–Poisson equation. The proposed approach involves an implicit Eulerian formulation in an augmented space – called field space, which incorporates both velocity and electric fields into the configuration. Both velocity and electric fields are captured through common zeros of two level set functions, which are governed by a field transport equation. Simultaneously we obtain a weighted density $f$ by solving again the field transport equation but with initial density as starting data. The averaged density is then resolved by the integration of the obtained $f$ against the Dirac delta-function of two level set functions in the field space. Moreover, we prove that such obtained averaged density is simply a linear superposition of all multi-valued densities; and the averaged field quantities are weighted superposition of corresponding multi-valued ones. Computational results are presented and compared with some exact solutions which demonstrate the effectiveness of the proposed method.


*Keywords:* Multi-valued solution; Level set method; Euler–Poisson equations

## 1. Introduction

The aim of this paper is to introduce a new field-space-based level set method for computing multi-valued solutions to the Euler–Poisson system

$$\partial_t \rho + \partial_x(\rho u) = 0, \quad x \in \mathbb{R},\ t > 0, \tag{1.1}$$

$$\partial_t u + u\partial_x u = KE, \tag{1.2}$$

$$\partial_x E = \rho - c(x). \tag{1.3}$$

These are equations of conservation of mass, Newton's second law, and the Poisson equation, respectively. Here $K$ is a physical constant, which indicates the property of forcing, i.e., repulsive when $K > 0$ and attractive

* Corresponding author.
*E-mail address:* hliu@iastate.edu (H. Liu).

0021-9991/$ - see front matter 
doi:10.1016/j.jcp.2006.12.018

when $K < 0$. And $\rho = \rho(t,x)$ is the local density, $u = u(t,x)$ is the mean velocity field, $E = E(t,x)$ is the electric field, and $c(x)$ is the background charge profile.

The Euler–Poisson system arises in many physical problems such as fluid dynamics, plasma dynamics, gaseous stars, quantum gravity and semiconductors, etc. As is known, the simple one-dimensional unforced inviscid Burgers' solution always forms a shock discontinuity, except for the nongeneric case of increasing initial profile, $u_0' \geqslant 0$. In contrast, it was shown in [11] that the corresponding Euler–Poisson system has global smooth solutions as long as its initial configuration is above a critical threshold, allowing a finite, negative velocity gradient. It was also shown for a sub-critical set of initial data, solutions of the Euler–Poisson system will develop singularity at a finite time. For Euler–Poisson equations, beyond singularity generalized solutions need to be chosen and interpreted to reflect the physical relevance. In some applications such as in fluid dynamics, a shock will develop after the singularity formation. But in other applications such as the semiclassical approximation of the Schrödinger–Poisson equation and the wave breaking in Klystrons [39], one must allow multi-valued solutions in order to capture physically relevant phenomena. The usual shock-capturing methods for computing entropy solutions do not give desired results.

The main goal in this work is to develop a novel level set method for computing multi-valued solutions to 1D Euler–Poisson equations. Previously in [38] we have identified a configuration space to unfold the multi-valuedness in both velocity and electric fields. This extended configuration space from the usual phase space is hence termed as the field space. In this work we further derive a procedure to evaluate multi-valued density and field quantities.

Our approach can be summarized as follows: we use a vector level set function $\Phi = (\phi_1, \phi_2)^\top \in \mathbb{R}^2$ in field space $(x,p,q) \in \mathbb{R}^3$ with $p = u(t,x)$ and $q = E(t,x)$ to describe dynamics of the 1D Euler–Poisson system (1.1)–(1.3). The vector level set function $\Phi = \Phi(t,x,p,q)$ is shown to satisfy the field transport equation

$$\partial_t \Phi + p\partial_x \Phi + Kq\partial_p \Phi - c(x)p\partial_q \Phi = 0.$$

The zero level set of this vector function, initiated as

$$\Phi_0(x,p,q) := (p - u_0(x), q - E_0(x))^\top,$$

forms a one-dimensional manifold in field space $(x,p,q) \in \mathbb{R}^3$: the interaction of two 2D manifolds $\{\phi_1 = 0\} \cap \{\phi_2 = 0\}$. This gives implicitly multi-valued velocity and electric fields through

$$(u,E) \in \{(p,q) | \Phi(t,x,p,q) = 0\}.$$

Note that $\Phi$ as a solution of the field transport equation is bounded in any domain where the initial velocity and electric fields are bounded.

We evaluate the density function by simultaneously solving the field transport equation for a new quantity $f$ near $\{(x,p,q); \Phi = 0\}$ but with initial density as starting data, i.e.,

$$\begin{aligned} &\partial_t f + p\partial_x f + Kq\partial_p f - c(x)p\partial_q f = 0, \\ &f(0,x,p,q) = \rho_0(x). \end{aligned}$$

The averaged density is thus resolved by the integration of $f$ against the Dirac delta-function of two level set functions in field space,

$$\bar{\rho}(t,x) = \int_{\mathbb{R}^2_{p,q}} f(t,x,p,q)\delta(\phi_1)\delta(\phi_2)\,\mathrm{d}p\,\mathrm{d}q.$$

We prove that such obtained averaged density is simply a linear superposition of all multi-valued densities, i.e.,

$$\bar{\rho}(t,x) = \sum_{i=1}^{N} \rho_i(t,x). \tag{1.4}$$

Moreover, the averaged velocity and electric fields can be further evaluated by

$$\bar{u} = \frac{\int_{\mathbb{R}^2} pf\delta(\phi_1)\delta(\phi_2)\,\mathrm{d}p\,\mathrm{d}q}{\bar{\rho}}, \tag{1.5}$$

$$\overline{E} = \frac{\int_{\mathbb{R}^2} qf\delta(\phi_1)\delta(\phi_2)\,\mathrm{d}p\,\mathrm{d}q}{\bar{\rho}}. \tag{1.6}$$

Regarding these two averaged quantities we have

$$\bar{u} = \frac{\sum_{i=1}^{N} u_i(t,x)\rho_i(t,x)}{\bar{\rho}}, \tag{1.7}$$

$$\overline{E} = \frac{\sum_{i=1}^{N} E_i(t,x)\rho_i(t,x)}{\bar{\rho}}, \tag{1.8}$$

where $(u_i, E_i)$ are multi-valued fields determined from our level set method.

We note that the Euler–Poisson system can be regarded as a semiclassical approximation of the nonlinear Schrödinger–Poisson equation

$$\mathrm{i}\epsilon\partial_t\psi^\epsilon = -\frac{\epsilon^2}{2}\partial_x^2\psi^\epsilon + KV^\epsilon\psi^\epsilon, \quad x \in \mathbb{R},\ t \geqslant 0, \tag{1.9}$$

$$\partial_x^2 V^\epsilon = c(x) - |\psi^\epsilon|^2, \tag{1.10}$$

where $\psi^\epsilon(\cdot,t)$ is a complex-valued wave function depending on the scaled Planck constant $\epsilon$, with $K$ being a scaled physical constant. This equation has been studied in different contexts, and in particular, as the fundamental equation in semiconductor applications, with $c > 0$ standing for the doping profile and $K \sim \lambda^{-2}$, $\lambda$ being the Debye number, consult [18] and references therein.

The electric field is determined by $E = -V_x$. Seeking the WKB-type solution of the form

$$\psi = \sqrt{\rho(t,x)}\exp(\mathrm{i}S(t,x)/\epsilon),$$

we recover, to the leading order when $\epsilon \ll 1$, the Euler–Poisson system (1.1)–(1.3) for $(\rho, u = S_x)$. We should mention that for one-dimensional case the passage from the Schrödinger–Poisson equation to the Euler–Poisson equation was proved in [37] for a set of sub-critical initial data, and the passage from the Schrödinger–Poisson equation to the Vlasov–Poisson equation was proved in [56] for more general initial data, see also [35,40] for earlier works.

For the Euler–Poisson system (1.1)–(1.3) itself, the authors in [11] showed that for $K > 0$ and $c(x) = 0$, the EP system (1.1)–(1.3) admits a global smooth solution if and only if

$$u_0'(\alpha) > -\sqrt{2K\rho_0(\alpha)}, \quad \forall\alpha \in \mathbb{R}.$$

Moreover,

$$\rho(x(\alpha,t)) = \frac{\rho_0(\alpha)}{\Gamma(\alpha,t)}, \quad \Gamma(\alpha,t) := 1 + u_0'(\alpha)(t) + \frac{K}{2}\rho_0(\alpha)t^2. \tag{1.11}$$

If the initial slope of $u_0$ is too negative, then the solution will breakdown at a finite time $t_c$,

$$t_c = \min_\alpha\{t, \Gamma(\alpha,t) = 0\},$$

beyond which multi-valued solutions should be sought. For the case of $K > 0$ and $c(x) = \mathrm{const} > 0$, the critical regularity condition becomes

$$|u_0'(\alpha)| < \sqrt{K(2\rho_0(\alpha) - c)}, \quad \forall\alpha \in \mathbb{R}.$$

Interestingly, if electric force becomes repulsive $K < 0$, the critical regularity condition reads

$$u_0'(\alpha) \geqslant \left(1 - \frac{\rho_0(\alpha)}{c}\right)\sqrt{-cK}, \quad \forall\alpha \in \mathbb{R}.$$

We note that parameterized solutions along particle trajectory remains valid if multi-valued solutions are considered. The solution formulas and the blowup time estimates obtained in [11] provide us a valuable guide when we check the accuracy and validity of our methods using various testing examples.

We also note that previously in [39] the authors evaluated averaged density of an Euler–Poisson system in Klystrons with a quite different approach, using Vlasov–Poisson equations in phase space to interpret the multi-valued solutions. We comment on this in Section 4. We refer to [22,23] for multi-phase semiclassical approximation of an electron in a 1D crystalline lattice using the K-branch solution approach [1].

From a broader perspective, numerical capturing of multi-valued solutions is important in many applications. Examples are the computation of dispersive waves [16,31–33,55], optical waves [10,12,13,20,36,42,46], seismic waves [17,49,53], semiclassical limits of Schrödinger equations [6,21,26,48], electron beam modulation in vacuum electronic devices [25,39], etc. In these applications when the wave field is highly oscillatory, direct numerical simulation of the wave dynamics can be prohibitively costly, and approximate models for wave propagation must be used. The resulting approximate models are often nonlinear, and classical entropy-type solutions, such as the viscosity solution introduced in [7], are not adequate in describing the wave behavior beyond the singularity, where multi-valued solutions in physical space should be sought. Techniques that have been suggested in literature include ODE-based Lagrangian methods, nonlinear Hamilton–Jacobi equation-based Eulerian methods.

A recent approach for improving physical-space-based Eulerian methods is the use of a kinetic formulation in phase space, consult [1,12] for its early use in the context of multi-phase computation for optical waves. There is, however, a serious drawback with direct numerical approximations of the kinetic equation which is the need for a large set of independent variables in the phase space. To remedy this problem, two ways are suggested in the literature. One is the moment method, which is based on reducing the number of independent variables by introducing equations for moments, see e.g. [1,12,21,26,46]. The other is based on computations of special wave front solutions. For tracking wave fronts in geometric optics, geometry based methods in phase space such as the segment projection method [14] and the level set method [9,42] have been recently introduced. Consult the seminal survey article [13] for recent development of computational high frequency wave propagation.

More recently, with a geometric point view in place of the kinetic one in phase space, a new level set method framework has been developed for computing multi-valued phases and other physical observables in the entire physical domain in [6,29,30,27,28]. The effective equations which have been studied include general nonlinear first-order equations [30] and weakly coupled WKB systems of the form

$$\partial_t S + H(x, \nabla_x S) = 0, \quad \partial_t \rho + \nabla_x \cdot (\rho \nabla_k H(x, \nabla_x S)) = 0,$$

with applications in the semiclassical approximation of Schrödinger equations $\left(H = \frac{1}{2}|k|^2 + V(x)\right)$ [6,27], geometrical optics limit of the wave equation ($H = c(x)|k|$) [28,43]. We note that for first-order quasi-linear hyperbolic equations, the level set formulation based on graph evolution was known much earlier, see e.g. [4]. We also refer to [5,8,10,36,43] for various developments of the phase-space-based level set method applied to the geometric optics. The use of level set formulation for computing discontinuous solutions to Hamilton–Jacobi equations is proposed in [52]. We refer to the recent review article [34] for the level set method and multi-valued solutions in computational high frequency wave propagation.

However, in the Euler–Poisson system (1.1)–(1.3) the second equation for velocity $u$ couples with the Poisson equation (1.3), hence phase-space-based level set methods introduced previously do not apply. The main novelty of our approach in this work is the use of field space in which the Lagrangian manifold is identified by $\Phi = 0$ and the dynamics of the Euler–Poisson system can be recast into a closed characteristic system along the particle trajectory in field space. Then the level set equation is just a transport equation with speed determined by the vector field of the characteristic system. Multi-valued velocity and electric fields are thus resolved as common zeros of two level set functions initiated as $(p - u_0(x))$ and $(q - E_0(x))$, respectively. A post-processing step described above enables us to evaluate the density and other physical observables.

The rest of this paper is organized as follows. In Section 2 we describe the field space method and level set formulations introduced in [38], which are crucial ingredients for evaluating the density. Section 3 is devoted to a derivation of the field transport equation for a new quantity $f$ as well as the justification of the integration procedure for computing the density. In Section 4 linear superposition principle for multi-valued $\rho$ is proved; Averaged field quantities are also shown to be a weighted superposition of corresponding multi-valued ones.

In Section 5 we discuss generalizations and possible connections with kinetic equations as well as the Schrödinger–Poisson equation. In Section 6 we present detailed numerical procedures for implementing the proposed method. Finally in Section 7 we describe the numerical strategy explored in this paper and present some numerical results to verify the capacity of our method.

## 2. Level set equation in field space

We recall the level set formulation derived in [38] for computing multi-valued velocity and electric fields for 1D Euler–Poisson equations (1.1)–(1.3), subject to the following initial conditions

$$\rho(0,x) = \rho_0(x), \quad u(0,x) = u_0(x). \tag{2.1}$$

In this model, $c(x) \geqslant 0$ denotes the fixed positively charged background, i.e. the doping profile in semiconductor modeling [41]. The initial electric field can be determined from the density, but in different way for cases, $c \neq 0$ and $c \equiv 0$, respectively.

As shown in [11], for Euler–Poisson equations, only a subset of initial configurations leads to global smooth solutions. For sub-critical initial data the classical solution will fail at finite time when particle trajectory collides. As pointed out in Section 1 beyond the singularity we are going to adopt and compute multi-valued solutions.

In order to capture multi-valued fields, we advocate a new method based on level set formulations in an augmented space. The augmented space we are taking is $(x,p,q) \in \mathbb{R}^3$ with $p = u$ and $q = E$, called the *field space* since it incorporates both velocity and electric fields. Instead of looking for explicit solutions in field space, we are seeking implicit solutions identified as a common zero of two implicit functions, in which multi-valued velocity and electric fields are implicitly represented.

We now sketch one derivation of the level set formulation by employing the given Euler–Poisson system. It is known that the electric field $E$ satisfies a forced transport equation, see [24,38],

$$E_t + uE_x = -c(x)u. \tag{2.2}$$

Let $\Phi(t,x,p,q) \in \mathbb{R}^2$ be a vector function and its Jacobian matrix $\det\left(\frac{\partial\Phi(t,x,p,q)}{\partial(p,q)}\right) \neq 0$, the implicit function theorem suggests that $\Phi(t,x,p,q) = 0$ may determine two functions $p = p(x,t)$ and $q = q(x,t)$, at least locally where the Jacobian matrix is nonsingular. Let $p = u(x,t)$ and $q = E(x,t)$ be a solution of the Euler–Poisson system, we thus obtain

$$\Phi(t,x,u(t,x),E(t,x)) \equiv 0, \quad (x,t) \in \mathbb{R} \times \mathbb{R}^+. \tag{2.3}$$

Differentiation of (2.3) with respect to $t$ and $x$ respectively gives

$$\Phi_t + \Phi_p u_t + \Phi_q E_t = 0,$$
$$\Phi_x + \Phi_p u_x + \Phi_q E_x = 0.$$

Multiplying $u$ to the second equation and adding to the first one results in the following:

$$\Phi_t + u\Phi_x + (u_t + uu_x)\Phi_p + (E_t + uE_x)\Phi_q = 0.$$

Applying $u = p$, $u_t + uu_x = KE$, and $E_t + E_x u = -c(x)u$ to the above equation, we obtain

$$\Phi_t + p\Phi_x + Kq\Phi_p - c(x)p\Phi_q = 0. \tag{2.4}$$

Note that this transport equation can also be written as in conservative form

$$\Phi_t + (p\Phi)_x + (Kq\Phi)_p - (c(x)p\Phi)_q = 0,$$

since the divergence of the velocity field in $(x,p,q)$ space is null.

The initial conditions of (2.4) can be chosen as

$$\phi_1(0,x,p,q) = p - u_0(x), \tag{2.5}$$
$$\phi_2(0,x,p,q) = q - E_0(x). \tag{2.6}$$

Note that the choice of initial condition is not unique. However the zero sets of selected level set functions should uniquely embed the given initial data $u_0$ and $E_0$.

As argued in [11] based on the physical principle, $E_0(x)$ needs to be determined from $\rho_0(x)$ according to whether the background charge is present. For $c \neq 0$, the electric field is given by

$$E(0,x) = \int_{-\infty}^{x} (\rho(\xi,0) - c(\xi))\,\mathrm{d}\xi, \tag{2.7}$$

and for $c \equiv 0$:

$$E(0,x) = \frac{1}{2}\left(\int_{-\infty}^{x} \rho(\xi,0)\,\mathrm{d}\xi - \int_{x}^{\infty} \rho(\xi,0)\,\mathrm{d}\xi\right). \tag{2.8}$$

## 3. Evaluation of density

Equipped with the obtained level set formulation for both velocity and electric fields in field space $(x,p,q) \in \mathbb{R}^3$, we now introduce an approach for capturing the multi-valued density $\rho$. Note that the density $\rho$ formally solves the mass equation in the physical space $(t,x) \in \mathbb{R}^+ \times \mathbb{R}$,

$$\partial_t \rho + u\partial_x \rho = -\rho u_x.$$

When the velocity field is multi-valued, the density is forced to become multi-valued too. Note that along the particle trajectory $x = x(t,\alpha)$, governed by $\frac{\mathrm{d}}{\mathrm{d}t}x = u(t,x)$ with $x(0) = \alpha \in \mathbb{R}$, we have

$$\rho(t,x(t,\alpha)) = \frac{\rho_0(\alpha)}{\Gamma(t,\alpha)},$$

where $\Gamma(t,\alpha) = \partial_\alpha x(t,\alpha)$ indicates the deformation of particle trajectories. The density would become unbounded at the instant $t_c$, $\Gamma(t_c,\alpha) = 0$, when the velocity field starts to become multi-valued. This difficulty makes a direct computation of $\rho$ unrealistic.

The strategy is to first derive an evolution equation for a density representative in field space $(x,p,q)$, and then project it onto the 1D Lagrangian manifold expressed implicitly by $\{(x,p,q)|\Phi = 0\}$, involving both velocity and electric fields.

Let $\tilde{\rho}(t,x,p,q)$ be a representative of $\rho(t,x)$ in field space, i.e.,

$$\rho(t,x) \equiv \tilde{\rho}(t,x,u(t,x),E(t,x)).$$

We thus have

$$\partial_t \rho + u\partial_x \rho = \partial_t \tilde{\rho} + u_t \partial_p \tilde{\rho} + E_t \partial_q \tilde{\rho} + u(\partial_x \tilde{\rho} + u_x \partial_p \tilde{\rho} + E_x \partial_q \tilde{\rho}) = [\partial_t + u\partial_x + (u_t + uu_x)\partial_p + (E_t + uE_x)\partial_q]\tilde{\rho}.$$

Using Eqs. (1.2) and (2.2) we have

$$\partial_t \rho + u\partial_x \rho = \partial_t \tilde{\rho} + u\partial_x \tilde{\rho} + KE\partial_p \tilde{\rho} - c(x)u\partial_q \tilde{\rho}.$$

Hence the density equation in the field space follows:

$$L\tilde{\rho} = -\tilde{\rho}\partial_x u, \tag{3.1}$$

where the field transport operator is defined as

$$L := \partial_t + p\partial_x + Kq\partial_p - c(x)p\partial_q.$$

The above observation, also true for other quantities, is summarized in the following:

**Lemma 3.1.** *Let $\tilde{w}(t,x,p,q)$ be a representative of $w(t,x)$ in field space such that*

$$w(t,x) = \tilde{w}(t,x,u(t,x),E(t,x)).$$

*Then*

$$\partial_t w + u\partial_x w = L\tilde{w}(t,x,p,q).$$

From (3.1), we still need to evaluate $u_x$ in field space in terms of the level set function $\Phi$. To this end we differentiate the level set equation, $L\Phi = 0$, with respect to $p$ and $q$ respectively and obtain

$$L(\partial_p \Phi) + (\partial_x - c(x)\partial_q)\Phi = 0,$$
$$L(\partial_q \Phi) + K\partial_p \Phi = 0.$$

Set

$$J = \det(\Phi_p \Phi_q) = \Phi_p \cdot \Phi_q^{\perp}, \quad \Phi^{\perp} := (\phi_2, -\phi_1)^{\top},$$

we have

$$L(J) = -\det(\Phi_x \Phi_q). \tag{3.2}$$

In fact

$$L(J) = L(\Phi_p)\cdot \Phi_q^{\perp} + \partial_p \Phi \cdot (L(\Phi_q))^{\perp} = (c\partial_q - \partial_x)\Phi \cdot \partial_q \Phi^{\perp} - K\partial_p \Phi \cdot (\partial_p \Phi)^{\perp} = -\partial_x \Phi \cdot \partial_q \Phi^{\perp}$$
$$= -\det(\Phi_x \Phi_q).$$

In order to express $u_x$ in (3.1) in terms of $\Phi$, we further differentiate the relation

$$\Phi(t, x, u(t,x), E(t,x)) = 0$$

with respect to $x$ to obtain

$$\partial_x \Phi + u_x \partial_p \Phi + E_x \partial_q \Phi = 0,$$

from which we obtain

$$u_x = -\frac{\det(\Phi_x \Phi_q)}{\det(\Phi_p \Phi_q)}.$$

This when inserted into (3.1) gives

$$L(\tilde{\rho}) = \tilde{\rho}\frac{\det(\Phi_x \Phi_q)}{J}. \tag{3.3}$$

Note that at the singular point, $J$ is zero and (3.3) is not defined, where integral equation should be considered. Following [27,28] for density evaluation from phase space, we evaluate the multi-valued density in physical space by projecting its value from field space $(x, p, q)$ onto the manifold $\Phi = 0$, i.e., for any $x$ we compute

$$\bar{\rho}(t,x) = \int_{\mathbb{R}_{p,q}} \tilde{\rho}(t,x,p,q)|J|\delta(\phi_1)\delta(\phi_2)\,\mathrm{d}p\,\mathrm{d}q.$$

Note that by the use of absolute value for $J$ is required since the Jacobian changes sign if singularities are formed.

A combination of (3.2) and (3.3) gives

$$L(\tilde{\rho}(\pm J)) = 0,$$

away from singularities. Then we have, away from the singular points,

$$L(f) = 0, \quad f := \tilde{\rho}|J|,$$

where the absolute sign is used to ensure the same nonnegative sign of $f$ before and after the blowup time when $J = 0$. Thus we just need to compute the quantity $f$ by solving the field transport equation

$$\partial_t f + p\partial_x f + Kq\partial_p f - c(x)p\partial_q f = 0, \tag{3.4}$$

subject to initial data

$$f(0,x,p,q) = \rho_0(x)J(0,x,p,q) = \rho_0(x). \tag{3.5}$$

Note that by choice of (2.5) and (2.6), $J(0,x,p,q) \equiv 1$. With this quantity $f$ the singularities in density $\rho$ is canceled out by $J(\Phi)$. Thus, we are able to locally evaluate the density in physical space by projection of $f$ onto the manifold $\{(p,q) : \Phi(x,p,q) = 0\}$

$$\bar{\rho}(t,x) = \int_{\mathbb{R}^2} f(t,x,p,q)\delta(\phi_1)\delta(\phi_2)\,\mathrm{d}p\,\mathrm{d}q. \tag{3.6}$$

Note that in field space the effective manifold for single valued fields is given by $\{(x,p,q)|p = u(t,x), q = E(t,x)\}$. For multi-valued velocity and electric fields, we have

$$(u,E) \in \{(p,q) : \phi_1(t,x,p,q) = 0, \phi_2(t,x,p,q) = 0\}.$$

We can evaluate their averages by

$$\bar{u}(t,x) = \int_{\mathbb{R}^2} pf(t,x,p,q)\delta(\Phi)\,\mathrm{d}p\,\mathrm{d}q/\bar{\rho}, \tag{3.7}$$

$$\overline{E}(t,x) = \int_{\mathbb{R}^2} qf(t,x,p,q)\delta(\Phi)\,\mathrm{d}p\,\mathrm{d}q/\bar{\rho}. \tag{3.8}$$

## 4. Superposition of multi-valued quantities

This section is devoted to the issue of how to relate the computed averaged physical observables such as $\bar{\rho}$, $\bar{u}$ and $\overline{E}$ to exact multi-valued quantities predicted by the characteristic method. We start with the observed mean density computed from the formula (3.6). We shall show that if multi-valued densities are given, the above calculated mean density is simply a superposition of all multi-valued densities. This result is summarized below.

**Theorem 4.1** (Superposition principle for the density). *Let* $\{\rho_i\}_{i=1}^N$ *be multi-valued densities corresponding to multi-valued fields* $(u_i,E_i)$ *determined by*

$$(u_i,E_i) \in \{(p,q) : \phi_l(t,x,p,q) = 0, l = 1,2\}.$$

*Then*

$$\bar{\rho}(t,x) = \sum_{i=1}^{N} \rho_i(t,x). \tag{4.1}$$

**Proof.** In order to evaluate the integral (3.6), we assume that all $(u_i,E_i)$ lie in a bounded domain and use a partition of unity so that we just need to evaluate

$$\int\int f\sigma\delta(\phi_1)\delta(\phi_2)\,\mathrm{d}p\,\mathrm{d}q,$$

where $\sigma \in C_0^\infty$ vanishes near $(p_i,q_i)$, with $\sigma(p_i,q_i) = 1$. Recall that for any smooth function $g(p)$ with only one zero $p = p^*$ we have

$$\delta(g(p)) = \frac{\delta(p-p^*)}{|g'(p^*)|}.$$

In the neighborhood of $(p_i,q_i)$, the implicit function theorem suggests that the zero level set $\phi_1 = 0$ can be explicitly expressed by $p = h(q)$ for each $q$ near $q_i$, with $p_i = h(q_i)$. Thus

$$\begin{aligned}\int\int f\sigma(p,q)\delta(\phi_1)\delta(\phi_2)\,\mathrm{d}p\,\mathrm{d}q &= \int\int f\sigma\frac{\delta(p-h(q))}{|\partial_p\phi_1|_{p=h(q)}}\delta(\phi_2)\,\mathrm{d}p\,\mathrm{d}q = \int\frac{f(t,x,h(q),q)\sigma(h(q),q)\delta(\phi_2(t,x,h(q),q))}{|\partial_p\phi_1|_{p=h(q)}|}\,\mathrm{d}q \\ &= \int\frac{f(t,x,h(q),q)\sigma(h(q),q)\delta(q-q_i)}{|\partial_p\phi_1|_{p=h(q)}\|\frac{\mathrm{d}}{\mathrm{d}q}\phi_2|_{q_i}}\,\mathrm{d}q = \frac{f(t,x,p_i,q_i)}{|\partial_p\phi_1\|\partial_p\phi_2h'(q)+\partial_q\phi_2|_{(p_i,q_i)}}.\end{aligned} \tag{4.2}$$

Furthermore, for any $q$ near $q_i$ we have

$$\phi_1(h(q), q) \equiv 0,$$

which leads to

$$\partial_p \phi_1 h'(q) + \partial_q \phi_1 = 0.$$

This when inserted into the denominator in (4.2) gives the Jacobian of $(\phi_1, \phi_2)$:

$$|\partial_p \phi_1 \partial_q \phi_2 - \partial_q \phi_1 \partial_p \phi_2| = |J|.$$

Note that $f(t, x, u_i, E_i) = \rho_i(t, x)|J|$, we thus have

$$\int\int f\sigma(p, q)\delta(\phi_1)\delta(\phi_2)\,\mathrm{d}p\,\mathrm{d}q = \rho_i(t, x).$$

This when combined with the partition of unity gives the asserted (4.1). □

This theorem shows that the linear superposition principle holds for the density of the nonlinear Euler–Poisson system in the sense that direct summation of all multi-valued densities gives the physical observed density. To our knowledge, this is the first rigorous proof via the field space configuration. It would be interesting to see whether this could be justified using the usual Wigner transform in the phase space.

Similar results hold for velocity and electric fields and are stated in the following.

**Theorem 4.2** (Weighted superposition for field quantities). *Let $\{\rho_i\}_{i=1}^N$ be multi-valued densities corresponding to multi-valued fields $(u_i, E_i)$ determined by*

$$(u_i, E_i) \in \{(p, q) : \phi_l(t, x, p, q) = 0, l = 1, 2\}.$$

*Then*

$$\bar{u}(t, x) = \frac{\sum_{i=1}^N u_i(t, x)\rho_i(t, x)}{\bar{\rho}}, \tag{4.3}$$

$$\overline{E}(t, x) = \frac{\sum_{i=1}^N E_i(t, x)\rho_i(t, x)}{\bar{\rho}}. \tag{4.4}$$

**Proof.** Replacing $f$ by $fp$ and $fq$ respectively in the proof of Theorem 4.1 we obtain the desired $\bar{u}$ and $\overline{E}$. □

Finally, we remark that the multi-valued quantities predicted by the characteristic method are nothing but those expressed implicitly by the zero level sets of $\phi_1$ and $\phi_2$ defined above.

## 5. Kinetic and quantum descriptions

In the following we discuss a kinetic formulation in field space for Euler–Poisson equations, and its connections with Schrödinger–Poisson equations, as well as Vlasov–Poisson equations in phase space.

### 5.1. Kinetic equation in field space

Since both $\Phi$ and $f$ solve a linear homogeneous transport equation (3.4), so does $\eta = f\delta(\Phi)$. For smooth initial velocity and electric fields, the density distribution $\eta$ thus evolves according to

$$\partial_t \eta + p\partial_x \eta + Kq\partial_p \eta - c(x)p\partial_q \eta = 0, \tag{5.1}$$

$$\eta(0, x, p, q) = \rho_0(x)\delta(p - u_0(x))\delta(q - E_0(x)). \tag{5.2}$$

This is a kinetic type equation in field space with nonnegative measure data. If we formally set

$$\rho = \int \eta\,\mathrm{d}p\,\mathrm{d}q, \quad \rho u^i E^j = \int p^i q^j \eta\,\mathrm{d}p\,\mathrm{d}q \quad 0 \leqslant i + j \leqslant 2.$$

Multiplying $\{1, p, q\}$ to (5.1) and integrating over $\mathbb{R}^2_{p,q}$ we obtain

$$\partial_t \rho + \partial_x(\rho u) = 0,$$
$$\partial_t(\rho u) + \partial_x(\rho u^2) - K\rho E = 0,$$
$$\partial_t(\rho E) + \partial_x(\rho u E) + c(x)\rho u = 0,$$

which, for smooth solutions, recovers the expected Euler–Poisson system (1.1), (1.2) and (2.2).

In order to recover (1.3), we let

$$W = E_x - (\rho - c).$$

By the choice of $E_0$ in (2.7) and (2.8), we have

$$W(0,x) = E_x(0,x) - \rho(0,x) + c = 0. \tag{5.3}$$

Using (1.1) and (2.2), we find that $W$ solves the following transport equation:

$$W_t + (uW)_x = 0. \tag{5.4}$$

By the uniqueness of the zero solution to (5.4) and (5.3), we conclude

$$W \equiv 0,$$

which gives (1.3).

### 5.2. Wigner transformation

Consider the one-dimensional Schrödinger–Poisson equation of the form

$$\mathrm{i}\epsilon\partial_t\psi^\epsilon = -\frac{\epsilon^2}{2}\partial_x^2\psi^\epsilon + V^\epsilon\psi^\epsilon, \quad x \in \mathbb{R},\ t \geqslant 0, \tag{5.5}$$
$$\partial_x^2 V^\epsilon = c(x) - |\psi^\epsilon|^2. \tag{5.6}$$

The electric field is determined by $E = -V_x$. Seeking the WKB-type solution of the form

$$\psi = \sqrt{\rho(t,x)}\exp(\mathrm{i}S(t,x)/\epsilon),$$

we obtain, to the leading order, the Euler–Poisson system for $(\rho, u = S_x)$, i.e., (1.1)–(1.3).

Another path for semiclassical approximation of quantum mechanics is to use the Wigner transformation from "physical space" into "phase space", which was introduced by Wigner [54] and can be written as

$$w^\epsilon(t,x,p) = \frac{1}{2\pi}\int_{\mathbb{R}} \mathrm{e}^{-\mathrm{i}py}\psi\left(t, x + \frac{\epsilon y}{2}\right)\overline{\psi\left(t, x - \frac{\epsilon y}{2}\right)}\,\mathrm{d}y.$$

We use the overbar to represent the complex conjugate. Wigner transform has been widely used in the study of high frequency, homogenization limits of various equations, see e.g. [19,45,23,35,48]. In the current setting, a direct calculation by applying the Wigner transform to the Schrödinger–Poisson system (5.5), (5.6) shows that $w^\epsilon(t,x,p)$ satisfies the so-called Wigner equation

$$\partial_t w^\epsilon + p\partial_x w^\epsilon + \theta^\epsilon[V^\epsilon]w^\epsilon = 0, \tag{5.7}$$

where the pseudo-differential operator (local in $x$ and nonlocal in $p$) is defined as

$$\theta^\epsilon[V^\epsilon]w^\epsilon := \frac{\mathrm{i}}{2\pi}\int\int \frac{V^\epsilon\left(x + \frac{\epsilon y}{2}\right) - V^\epsilon\left(x - \frac{\epsilon y}{2}\right)}{\epsilon} w^\epsilon(t,x,\xi)\mathrm{e}^{-\mathrm{i}(p-\xi)y}\mathrm{d}\xi\,\mathrm{d}y.$$

The macroscopic density $\rho(t,x)$ is usually computed through the zero moment in the kinetic variable $p$

$$\rho^\epsilon(t,x) = \int w^\epsilon(t,x,p)\,\mathrm{d}p.$$

Formally passing $\epsilon \to 0$ in the quantum Wigner Eq. (5.7) one obtains the Vlasov–Poisson system

$$\partial_t w + p\partial_x w + KE\partial_p w = 0, \quad K = 1, \tag{5.8}$$

$$E_x = \int_{\mathbb{R}_p} w(t,x,p)\,\mathrm{d}p - c(x). \tag{5.9}$$

For the WKB type initial data

$$\psi_0(x) = \sqrt{\rho_0(x)}\exp(\mathrm{i}S_0(x)/\epsilon),$$

the limit of the corresponding Wigner function becomes

$$w_0(x,p) = \rho_0(x)\delta(p - u_0(x)).$$

The classical limit from the Schrödinger–Poisson to the Vlasov–Poisson equations in one-dimensional case has been justified by Zhang et al. [56] for bounded integrable data. This V–P system is also a model for collisionless plasma of ions and corresponding electrons. The transport is uni-directional so that the problem can be formulated in one-space dimension. Here the particle motion is governed solely by induced electrostatic forces, while electromagnetic interactions are neglected.

In contrast the classical moment closure approach offers

$$\bar{\rho} = \int w\,\mathrm{d}p, \quad \overline{\rho u} = \int pw\,\mathrm{d}p.$$

In an interesting earlier work [39], the authors propose a moment closure approach based on the Vlasov–Poisson equation (5.8). From our study in [38] and in this work, we see that the electric field $E$ generally becomes multi-valued simultaneously with velocity field except in the case with null background. Thus solving problem (5.1), (5.2) in field space serves as an appropriate kinetic formulation to interpret multi-valuedness encountered.

### 5.3. From field space to phase space

We may also formally derive the Vlasov–Poisson equation from (5.1), (5.2). Assume the closure assumption as $\eta = w(t,x,p)\delta(q - E(t,x))$ we set

$$w(t,x,p) = \int \eta\,\mathrm{d}q, \quad E^i w(t,x,p) = \int q^i \eta\,\mathrm{d}q, \qquad i = 1,2.$$

Integration of the $\eta$-equation (5.1) against $\{1, q\}$ leads to

$$\partial_t w + p\partial_x w + KE\partial_p w = 0,$$

$$\partial_t(Ew) + p\partial_x(Ew) + K\partial_p(E^2 w) + c(x)pw = 0.$$

The combination of the two gives

$$\partial_t E + p\partial_x E + c(x)p = 0,$$

this coincides with (2.2) when projection onto the physical space is via $p = u(t,x)$.

## 6. Numerical procedures and implementation

In this section we discuss the numerical procedures of the new field-space-based level set method.

High dimension level set method was studied in [2] for motion of curves.

The main task encountered in this work is to evaluate the density $\bar{\rho}$ accurately. Based on the level set formulation, for evaluation of the density

$$\bar{\rho}(t,x) = \int_{\mathbb{R}_q}\int_{\mathbb{R}_p} f(t,x,p,q)\delta(\phi_1)\delta(\phi_2)\,\mathrm{d}p\,\mathrm{d}q, \tag{6.1}$$

we need to first compute two level set functions $\phi_1$, $\phi_2$ and the function $f$, all solve the field transport Eq. (2.4) of the compact form

$$\Phi_t + \overrightarrow{V}(X) \cdot \nabla_X \Phi = 0, \quad t \in \mathbb{R}^+, \ X \in \mathbb{R}^3, \tag{6.2}$$

where $X = (x, p, q)$ and

$$\overrightarrow{V} = (V_1, V_2, V_3) = (p, Kq, -c(x)p).$$

The initial data are chosen to embed the given initial data of the Euler–Poisson equation. One simple choice is

$$\Phi|_{t=0} = (p - u_0(x), q - E_0(x), \rho_0(x))^\top$$

for smooth $u_0$, $E_0$. Following [38], we discretize the gradient $\nabla_X \Phi$ by a first-order upwind approximation or a higher order ENO approximation [47], and then discretize time by a forward Euler method or a higher order Runge–Kutta method. Let $\{t_n, x_i, p_j, q_k\}$ be uniform grids in the $tX-$plane with mesh sizes $\Delta t$, $\Delta x$, $\Delta p$ and $\Delta q$, respectively. The simplest first-order upwind scheme can be formulated as

$$\frac{\Phi^{n+1}_{(i,j,k)} - \Phi^n_{(i,j,k)}}{\Delta t} + V_1(i,j,k)\Phi^{\pm}_x + V_2(i,j,k)\Phi^{\pm}_p + V_3(i,j,k)\Phi^{\pm}_q = 0, \tag{6.3}$$

where $\Phi^n_{(i,j,k)} \approx \Phi(t_n, x_i, p_j, q_k)$, $V_m(i,j,k) := V_m(x_i, p_j, q_k)$ $(m = 1,2,3)$ and

$$\Phi^+_x = \frac{\Phi^n_{(i+1,j,k)} - \Phi^n_{(i,j,k)}}{\Delta x}, \quad \Phi^-_x = \frac{\Phi^n_{(i,j,k)} - \Phi^n_{(i-1,j,k)}}{\Delta x},$$

similar notations are adopted for $\Phi^+_p$, $\Phi^-_p$, $\Phi^+_q$ and $\Phi^-_q$. For $m = 1, 2$ or 3, if $V_m(i,j,k) > 0$, we use $\Phi^-$; otherwise, $\Phi^+$ is applied. Under the CFL condition

$$\Delta t \max\left(\frac{|V_1|}{\Delta x} + \frac{|V_2|}{\Delta p} + \frac{|V_3|}{\Delta q}\right) \leqslant 1, \tag{6.4}$$

this scheme is stable in both $L^\infty$ and $L^1$ norm, which, to be stated below, were shown in [38] for more general $V$.

- [**Discrete Maximum Principle**] Assume that $V_m(x,p,q)$ $(m = 1,2,3)$ are bounded functions in the computational domain. Let $\Phi^n$ be a numerical solution produced by the first-order upwind scheme subject to the initial data $\Phi^0$, then

$$\|\Phi^n\|_\infty \leqslant \|\Phi^0\|_\infty. \tag{6.5}$$

- [$\mathbf{L^1}$ **Stability**] Assume that $V_m(x,p,q)$ $(m = 1,2,3)$ are bounded and Lipschitz continuous in its $i$th argument in the computational domain. Let $\Phi^n$ be a numerical solution produced by the first-order upwind scheme subject to the initial data $\Phi^0$, then for finite time $T$, there exists a constant $M$, such that

$$\|\Phi^n\|_1 \leqslant e^{MT}\|\Phi^0\|_1, \tag{6.6}$$

where $\|\Phi^n\|_1 := \sum_{i,j,k} |\Phi^n_{(i,j,k)}| \Delta x \Delta p \Delta q$.

In our numerical simulation, this first-order upwind scheme is mostly adopted for computing $\Phi = (\phi_1, \phi_2, f)^\top$, with which we discuss the evaluation of density via (6.1).

Since the integration (6.1) involves the Dirac $\delta$-function in its integrand, as usual we first regularize the Dirac $\delta$-function by a smooth bounded function $\delta_\epsilon$ in such a way that $\delta_\epsilon \rightharpoonup \delta$ as $\epsilon \to 0^+$. The error introduced in this regularization step depends on the choice of the approximation, whose accuracy is indicated by a so-called moment condition [3] of the regularization. $\delta_\epsilon$ is said to satisfy $r$th order of moment condition if $\int_{\mathbb{R}} \delta_\epsilon(x) = 1$ and $\int_{\mathbb{R}} \delta_\epsilon(x) x^k = 0$ for $1 \leqslant k \leqslant r$. It is known that the higher the order of moment condition, the smaller the regularization error. The choice of regularization $\delta_\epsilon$ could be any smooth function with the above properties. However, considering the concentration of the Delta function, it suffices to choose $\delta_\epsilon$ to have a compact support:

$$\delta_\epsilon(x) = \begin{cases} \frac{1}{\epsilon}\Psi(\frac{x}{\epsilon}), & |x| \leqslant \epsilon, \\ 0, & |x| > \epsilon. \end{cases}$$

One of well accepted choices of this type of $\delta_\epsilon$ is the cosine kernel, $\Psi(\eta) = \frac{1}{2}(1+\cos(\pi\eta))$, i.e.,

$$\delta_\epsilon^{\cos}(x) = \frac{1}{2\epsilon}\left(1+\cos\left(\frac{\pi x}{\epsilon}\right)\right) I_{[-\epsilon,\epsilon]}, \tag{6.7}$$

which has first-order moment condition. Here $I_{[-\epsilon,\epsilon]}$ is the standard indicator function.

Replacing $\delta(\phi_1)\delta(\phi_2)$ by $\delta_\epsilon(\phi_1)\delta_\epsilon(\phi_2)$, we thus have the first approximation of $\bar\rho$,

$$\bar\rho_\epsilon(t,x) = \int_{\mathbb{R}_q}\int_{\mathbb{R}_p} f(t,x,p,q)\delta_\epsilon(\phi_1)\delta_\epsilon(\phi_2)\,\mathrm{d}p\,\mathrm{d}q, \tag{6.8}$$

to which standard quadrature rules can be applied. In our simulation, the rectangle rule is chosen and the numerical density is further evaluated by

$$\bar\rho_{\epsilon h}(t,x) = \sum_{\{|\phi_i(t,x,p_j,q_k)|\leqslant\epsilon, i=1,2\}} f(t,x,p_j,q_k)\delta_\epsilon^{\cos}(\phi_1)\delta_\epsilon^{\cos}(\phi_2)\Delta p\Delta q. \tag{6.9}$$

In this two-step procedure, total error is bounded by the sum of regularization error $|\bar\rho - \bar\rho_\epsilon|$ and quadrature error $|\bar\rho_\epsilon - \bar\rho_{\epsilon h}|$. For example, if the cosine kernel and the rectangle rule are used, $|\bar\rho - \bar\rho_\epsilon|$ is of order $\epsilon$ and $|\bar\rho_\epsilon - \bar\rho_{\epsilon h}|$ is of order $h/\epsilon$, where $h = \max\{\Delta x, \Delta p, \Delta q\}$. Using the similar analysis as in [44], it is clear that the total error is minimized as of order $\sqrt{h}$ when an optimal $\epsilon^*$ is chosen to be of order $\sqrt{h}$. Thus the convergence rate of the numerical integration is at least of order 1/2, i.e.,

$$|\bar\rho - \bar\rho_{\epsilon h}| \leqslant Ch^{\frac{1}{2}}$$

for some constant $C$. For details on convergence rates in general cases, see [50, Theorem 3].

Though, theoretically, $\epsilon^*$ is optimal, it is impractical to determine it exactly. Thus, we choose to run numerical experiments with a wide range of $\epsilon$ to circumvent this numerical difficulty. In our simulation the support of $\delta_\epsilon$ is tested with $\epsilon = h, 2h, 3h, \ldots$ Based on many experiments on $\epsilon$, we found that the smaller $\epsilon$, the sharper of density at the cost of oscillation. So we have to pick proper $\epsilon$ to balance the resolution and smoothness. Through our simulation, we also found that usually we get best results when $\epsilon$ is within $[1.5h, 4.5h]$ depending on examples being tested. In short, the choice of $\epsilon$ plays a crucial role in the evaluation of density. An interesting phenomenon is that the choice of $\epsilon$ as $mh$ while using the signed distance function in multi-dimensional setting may lead to O(1) error [51]. However, in our case, a product of $\delta$-functions is being approximated. Thus convergence is guaranteed with $\epsilon^* \in [h, mh]$ for some constant $m$. We also notice that the geometry of the level set function also affects the choice of $\epsilon$, as observed in [27,28]. And we refer to [15] for more regularization techniques related to level set methods.

Here we remark that one could also compute the density $\bar\rho$ by solving the field transport equation (5.1):

$$\partial_t\eta + p\partial_x\eta + Kq\partial_p\eta - c(x)p\partial_q\eta = 0,$$

but subject to initial data involving delta functions,

$$\eta(0,x,p,q) = \rho_0(x)\delta(p-u_0(x))\delta(q-E_0(x)). \tag{6.10}$$

The density is then evaluated by

$$\bar\rho = \int \eta\,\mathrm{d}p\,\mathrm{d}q. \tag{6.11}$$

Here, $\bar\rho$ is still evaluated by a post-processing step, i.e. integration over field configuration, but with no involvement of the Dirac $\delta$-function. However, in order to utilize (6.11), one needs to regularize the $\delta$-function in the initial condition (6.10), and such an initial regularization error will surely evolve and accumulate, reducing accuracy of the final integration. Therefore, the evaluation of $\bar\rho$ by post-processing in (6.9) is preferred to solving the kinetic equation with (6.10) directly.

We now discuss several technical details to be involved in our numerical tests.

Firstly, we need to specify an appropriate computational domain.

The guiding principle is that the extreme values of $u$ and $E$ should be covered in the computation domain. Thus, if the example has an exact solution, we choose to prescribe a domain containing the range of the exact solution for all $t$ before the desired time $T$. In the case of no exact solution available, based on the initial condition, we first choose a relatively large domain with coarse meshes to get a rough solution in order to determine the computation domain. Then we can refine our mesh to get better resolution.

Secondly, the computational boundary condition should be enforced in such a way that no artificial and spurious waves are propagated into the computational domain. In our simulation, if the initial data are periodic in an argument, we use a periodic boundary data in the direction of that argument. For other cases, we use a Neumann boundary condition.

Finally, we show how to realize multi-valued $u$ and $E$. The projection of common zeros onto $xp$ and $xq$ spaces gives the visualization of multi-valued $u(T,x)$ and $E(T,x)$:

$$(u,E)(T,x) \in \{(p,q)|\phi_1(T,x,p,q)=0\} \cap \{(p,q)|\phi_1(T,x,p,q)=0\}, \quad \forall x \in \mathbb{R}.$$

Numerically, we interpolate only grid points satisfying

$$\{(x_i,p_j,q_k) \in \Omega|\ |\phi_1(T,x_i,p_j,q_k)| < \tilde{\epsilon},\ |\phi_2(T,x_i,p_j,q_k)| < \tilde{\epsilon}\},$$

where $\tilde{\epsilon}$ is chosen in such a way that a unique grid point can be identified along the zero level set. Computationally, a $\tilde{\epsilon}$ which is much smaller than $h$ works well. We point out that a larger $\tilde{\epsilon}$ may be necessary for the case when level set functions are rough. Meanwhile the density $\bar{\rho}$ is approximated by (6.9) using $\phi_1$ and $\phi_2$.

Using the multi-valued density predicted by the characteristic method and the superposition principle (4.1), we construct an exact averaged density

$$\bar{\rho}_{ea} = \sum_{i=1}^{N} \rho_i(t,x). \tag{6.12}$$

Based on this, we show the numerical accuracy and convergence for averaged density obtained by our level set method (6.9).

Numerical convergence test with $L^2$ error of (6.9) and (6.12) is performed.

### 6.1. Exact solution and breakdown time

We now recall some solution formulas given in [11] by using the characteristic system

$$\frac{\mathrm{d}x}{\mathrm{d}t} = u, \tag{6.13}$$

$$\frac{\mathrm{d}u}{\mathrm{d}t} = KE, \tag{6.14}$$

$$\frac{\mathrm{d}E}{\mathrm{d}t} = -c(x)u \tag{6.15}$$

of (1.1)–(1.3) subject to the initial condition

$$x(0) = \alpha, \quad u(0) = u_0(\alpha), \quad E(0) = E_0(\alpha).$$

1. Zero background charge $c(x) \equiv 0$.

Integration of the characteristic system (6.13)–(6.15) leads to

$$x(t,\alpha) = \alpha + u_0 t + KE_0 t^2/2, \tag{6.16}$$

$$u(t,x(t,\alpha)) = u_0 + KE_0 t, \tag{6.17}$$

$$E(t,x(t,\alpha)) = E_0. \tag{6.18}$$

The density is conserved along characteristics, see (1.11). As shown in [11], the necessary and sufficient condition for the break down of smooth solution is $\Gamma(t,\alpha)=0$ for some time $t$ and initial position $\alpha$. This condition also gives the exact time when breakdown occurs, which in current setting gives

$$T^*=\min_{\alpha}\left\{t:\frac{-u_0'-\sqrt{u_0'^2-2K\rho_0}}{K\rho_0},\ u_0'<-\sqrt{2K\rho_0}\right\}, \tag{6.19}$$

where $\{\alpha: u_0'<-\sqrt{2K\rho_0}\}$ denotes the set of initial points which will lead to finite time breakdown.

2. Constant background charge $c>0$.

By the characteristic Eqs. (6.14) and (6.15), we have

$$u''+cKu=0.$$

If the force is repulsive, $K>0$, solutions are

$$x(t,\alpha)=\alpha+u_0\sin\left(\sqrt{cK}t\right)+E_0\cos\left(\sqrt{cK}t\right)-E_0, \tag{6.20}$$

$$u(t,x(t,\alpha))=u_0\cos\left(\sqrt{cK}t\right)+E_0\sin\left(\sqrt{cK}t\right), \tag{6.21}$$

$$E(t,x(t,\alpha))=E_0\cos\left(\sqrt{cK}t\right)-u_0\sin\left(\sqrt{cK}t\right), \tag{6.22}$$

where the density is still given by $\rho(t,x(t,\alpha))=\frac{\rho_0(\alpha)}{\Gamma(t,\alpha)}$, but with

$$\Gamma(t,\alpha)=1+u_0'\sin\left(\sqrt{cK}t\right)+E_0'\cos\left(\sqrt{cK}t\right)-E_0'. \tag{6.23}$$

Finite time breakdown is unavoidable if

$$|u_0'(\alpha)|\geqslant\sqrt{K(2\rho_0-c)}$$

for some $\alpha\in\mathbb{R}$. Under this condition, the first breakdown time is

$$T^*=\min_{\alpha}\left\{t,\Gamma(t,\alpha)=0,|u_0'(\alpha)|\geqslant\sqrt{K(2\rho_0-c)}\right\}.$$

If the force is attractive, i.e. $K<0$, then

$$x(t,\alpha)=\alpha+\frac{C_1}{-\lambda}(e^{-\lambda t}-1)+\frac{C_2}{\lambda}(e^{\lambda t}-1), \tag{6.24}$$

$$u(t,x(t,\alpha))=C_1e^{-\lambda t}+C_2e^{\lambda t}, \tag{6.25}$$

$$E(t,x(t,\alpha))=\frac{-C_1\lambda}{K}e^{-\lambda t}+\frac{C_2\lambda}{K}e^{\lambda t}, \tag{6.26}$$

$$\rho(t,x(t,\alpha))=\frac{\rho_0(\alpha)}{\Gamma(t,\alpha)}, \tag{6.27}$$

where $\lambda=\sqrt{-cK}$, $C_1=\frac{\lambda u_0-E_0K}{2\lambda}$, $C_2=\frac{\lambda u_0+E-0K}{2\lambda}$ and

$$\Gamma(t,\alpha)=1+\frac{C_1'}{-\lambda}(e^{-\lambda t}-1)+\frac{C_2'}{\lambda}(e^{\lambda t}-1).$$

In this case, the necessary and sufficient condition for smooth solutions to experience finite time breakdown is

$$u_0'(\alpha)\leqslant-\left(1-\frac{\rho_0(\alpha)}{c}\right)\sqrt{-Kc}$$

for some $\alpha\in\mathbb{R}$. Under this condition, $T^*$ can be found by solving $\Gamma(t,\alpha)=0$.

These parameterized solution formulas give multi-valued solutions of $u$, $E$ and $\rho$ after interaction of characteristic curves, i.e. $t>T^*$. Thus, we can compare our numerical solution with exact solutions to verify the accuracy of our method.

## 7. Numerical examples

In this section, we demonstrate the accuracy and capacity of our level set method by testing several numerical examples and compare the numerical solution with the parameterized exact solution when available. In the following experiments, the first-order upwind scheme is employed.

### 7.1. Numerical test one: 5 branches

Our first example is the model with zero background with $c = 0$, $K = 0.01$. The initial condition is given by

$$u(0,x) = \sin^3(x),$$
$$\rho(0,x) = \frac{1}{\pi} e^{-(x-\pi)^2}.$$

In this case, since $c$ is zero, the initial electric field $E_0(x)$ is determined from $\rho_0(x)$ by

$$E_0(x) := E(0,x) = \frac{1}{2}\left(\int_{-\infty}^{x} \rho_0 \, dx - \int_{x}^{-\infty} \rho_0 \, dx\right).$$

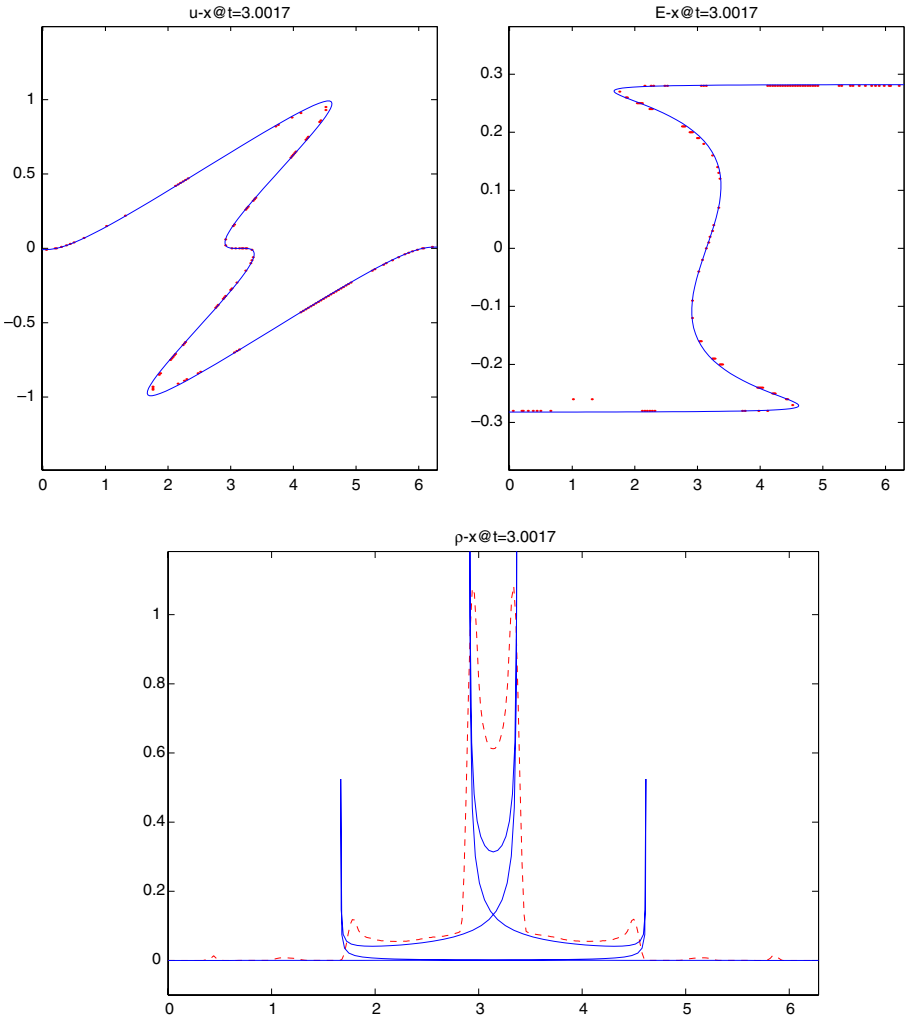


Fig. 1. Multi-valued solution for 1D Euler–Poisson equation at time about 3.

In this example, (1.11) gives

$$\Gamma(t,\alpha) = 1 + 3\sin^2(\alpha)\cos(\alpha)t + \frac{1}{2\pi}Kt^2 e^{-(\alpha-t)^2}.$$

A calculation based on (6.19) shows that $T^* < 3$. So we compare our numerical results with exact solution at time $t$ after 3. Our computation domain is $\Omega = [0, 2\pi] \times [-1.2, 1.2] \times [-0.5, 0.5]$, which is chosen to include the range of $u, E, \rho$ at $t \approx 3$. The discretization parameters $\Delta x,\ \Delta p,\ \Delta q$ are chosen to be 0.02, 0.01, 0.01 respectively, with $\tilde{\epsilon} = 0.0025$, $\epsilon = 1.5\Delta x$ and CFL number 0.8.

In Fig. 1 and other following figures, unless specified otherwise, solid line is exact solution while dots are our numerical results. We see that results from our level set method match the exact solution, though only a first-order upwind scheme has been used.

Now, we perform the numerical convergence test for the averaged density. $\bar{\rho}_{\epsilon h}$ is calculated with $\epsilon = mh$ via (6.9) for $m = 1, 2, 3, 4$. Then the numerical $L^2$ error between $\bar{\rho}_{\epsilon h}$ and $\bar{\rho}_{ea}$ obtained in (6.12) is computed as

$$\int (\bar{\rho}_{ea} - \bar{\rho}_{\epsilon h})^2 \,\mathrm{d}x \approx \sum_{\{x_i\}} (\bar{\rho}_{ea}(t, x_i) - \bar{\rho}_{\epsilon h}(t, x_i))^2 \Delta x.$$

In Table 1, one sees that the $L^2$ error becomes small as the step size decreases for some selected $\epsilon$. This is also visually shown in Fig. 2. Thus the numerical convergence is obtained, which shows the validity of our level set approach in computing averaged density.

### 7.2. Numerical test two: 7 branches

We now test the model with zero background with $c = 0$, $K = 0.01$, but subject to initial condition,

$$u(0,x) = \sin(2x)\cos(x),$$
$$\rho(0,x) = \frac{1}{\pi} e^{-(x-\pi)^2}.$$

Though this example is similar to the first one, the solution has richer structures. Note that from the numerical convergence test in example 1, we are assured that the level set approach developed here will give correct multi-valued $u$, $E$ and averaged $\bar{\rho}$. Thus from this example on, we choose not to do the numerical convergence test. Instead, we will just show the averaged density obtained from the level set method, and exact multi-valued density predicated by the characteristic method.

As in the first example, the initial condition $E_0(x)$ is given by

$$E_0(x) = \frac{1}{2}\left(\int_{-\infty}^{x} \rho_0 \,\mathrm{d}x - \int_{x}^{-\infty} \rho_0 \,\mathrm{d}x\right).$$

Table 1
$L^2$ error for averaged density at various spatial step sizes and support $\epsilon = mh$

| $\{\mathrm{d}x, \mathrm{d}p, \mathrm{d}q, t\}$ | $m$ | $L^2$ error |
|---|---|---|
| {0.06, 0.03, 0.03, 3.0149} | 1 | 0.1018 |
| | 2 | 0.1345 |
| | 3 | 0.1464 |
| | 4 | 0.1693 |
| {0.05, 0.02, 0.02, 3.0021} | 1 | 0.0513 |
| | 2 | 0.0714 |
| | 3 | 0.0790 |
| | 4 | 0.0901 |
| {0.02, 0.01, 0.01, 3.0017} | 1 | 0.0412 |
| | 2 | 0.0626 |
| | 3 | 0.0776 |
| | 4 | 0.0895 |

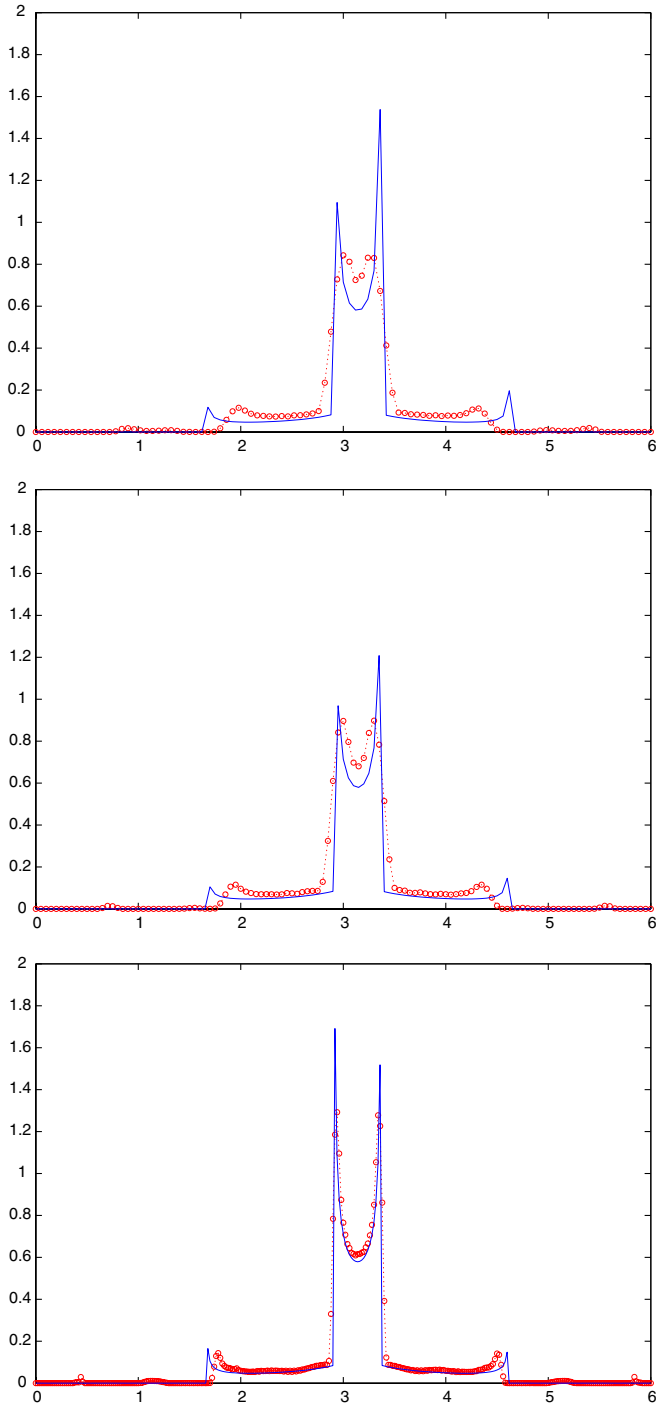


Fig. 2. Comparison of averaged $\rho_{eh}$ (dash and circle) and $\rho_{ea}$ (solid) at various spatial step size and time about 3. Spatial step size decreases from top to bottom as in Table 1.

Then the exact solution can be found using (6.16) and (1.11).

Using the same formula (6.19) as in the previous example in determining the critical time $T^*$, we find that multi-valued solution will appear before $t = 4$. Our computation domain is $\Omega = [0, 2\pi] \times [-1, 1] \times [-0.5, 0.5]$,

which is chosen to include the range of $u,\ E,\ \rho$ at desired time. The discretization parameters $\Delta x,\ \Delta p,\ \Delta q$ are chosen to be $0.02,\ 0.01,\ 0.01$ respectively, with $\tilde{\epsilon} = 0.0025$, $\epsilon = 4.5\Delta x$ and CFL number 0.8.

In Fig. 3, once again, by comparing with the exact solution, we see that results from our level set method match the exact solution. In this example, when we used smaller $\epsilon$, some oscillations for $x \in [2, 4]$ are observed. Thus, we pick relatively bigger $\epsilon = 4.5\Delta x$ to smear the observed oscillation.

### 7.3. Numerical test three: Negative K

In the previous two examples, multi-valuedness is induced by the decreasing initial velocity in finite time. However, if the force is attractive, $K < 0$, even for constant initial velocity, breakdown still occurs at finite time. This can be seen from the following example. If we consider zero background case, i.e. $c = 0$, the solution for $x$ and $\Gamma$ are given by

$$x(t,\alpha) = \alpha + u_0(\alpha)t + E_0(\alpha)Kt^2/2,$$
$$\Gamma(t,\alpha) = 1 + u_0'(\alpha)t + \rho_0 Kt^2/2.$$

Thus even if $u_0(\alpha)$ is nondecreasing, as long as $K$ is negative, there will be some time $t$ such that $\Gamma = 0$ provided that $\rho_0 \geqslant 0$. This tells us that multi-valued solutions must appear in the case of $K < 0$.

Now we test our method with $c = 0$ and $K = -1$, subject to initial condition,

$$u(0,x) = 0.01,$$
$$\rho(0,x) = \frac{1}{\pi} e^{-(x-\pi)^2}.$$

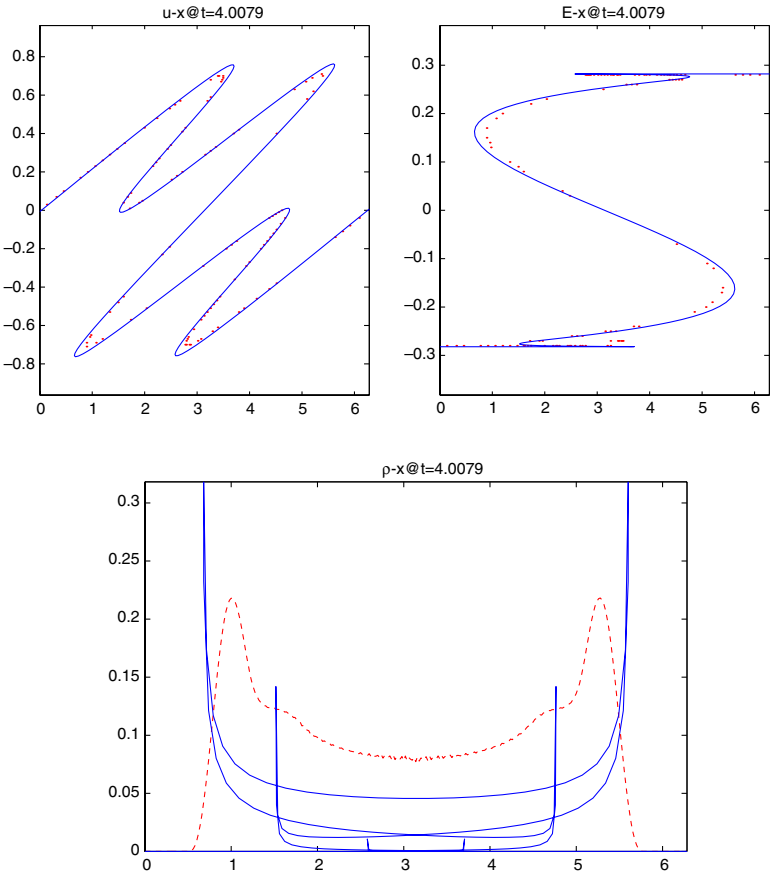


Fig. 3. Multi-valued solution for 1D Euler–Poisson equation at $t = 4.0079$.

In this case, $\Gamma = 1 - \frac{1}{2\pi} e^{(\alpha-\pi)^2} t^2$, which starts to become zero at $\alpha = \pi$, $t = T^* = \sqrt{2\pi}$. Thus when $t > \sqrt{2\pi}$, multi-valued solutions need to be considered. In order to see more structures, we will test our algorithm at time $t$ around 4. Our computation domain is $\Omega = [0, 2\pi] \times [-1.5, 1.5] \times [-0.5, 0.5]$, which is chosen to include the range of $u$, $E$, $\rho$ at desired time. The discretization parameters $\Delta x$, $\Delta p$, $\Delta q$ are chosen to be 0.02, 0.01, 0.01 respectively, with $\tilde{\epsilon} = 0.002$, $\epsilon = 1.5\Delta x$ and CFL number 0.8. In Fig. 4, we see that though the structure of the solution is not so rich as in previous one, this example does validate the physical situation that attractive force always induces multi-valued solutions in finite time.

### 7.4. Numerical test four: nonzero background

We now test an example with nonzero background with $c = 1$, $K = 1$ and initial condition,

$$u(0, x) = 2 \sin^4 x,$$
$$\rho(0, x) = 1.$$

In this case, as in (6.20)–(6.23) the exact solution can be found explicitly. Here the choice of constant initial density is to simplify the identification of when multi-valuedness happens. Since $\Gamma(t, \alpha) = 1 + 4 \sin\alpha \sin 2\alpha \sin t$,

$$T^* = \min_{\alpha} \sin^{-1}\left\{-\frac{1}{4 \sin 2\alpha \sin^2 \alpha}\right\} \approx 0.5.$$

We visualize our numerical simulation at $t = 1$. Our computation domain is $\Omega = [0, 2\pi] \times [-2.5, 2.5] \times [-2.5, 2.5]$, which is chosen to include the range of $u$, $E$, $\rho$ at desired time. The discretization parameters

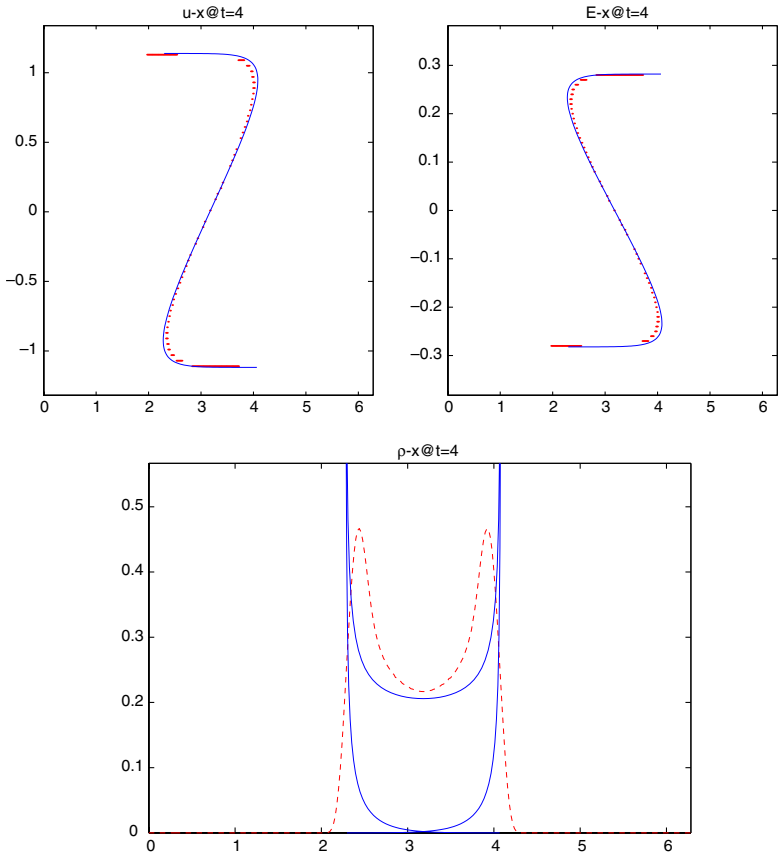


Fig. 4. Multi-valued solution for 1D Euler–Poisson equation at time around 4.

$\Delta x,\ \Delta p,\ \Delta q$ are chosen to be 0.02, 0.02, 0.02 respectively, with $\tilde{\epsilon} = 0.01$, $\epsilon = 2.5\Delta x$ and CFL number 0.8. In Fig. 5, we see the results in two periods. Looking at the graph for $\rho$ at $x$ near $2\pi$, one may wonder why the peak is not complete. This is caused by the fact that the wave is shifting to right while our computation domain is fixed in $[0, 4\pi]$.

### 7.5. Numerical test five: discontinuous background $c(x)$

In previous examples, all parameters and initial conditions are smooth. Thus the exact solution can be expressed in terms of the initial position parameter $\alpha$. By comparing with exact solution within the same graph, we have verified the accuracy of our method.

We now present an example with piecewise smooth background charge.

Consider the model with discontinuous background with $c = \frac{1}{2} I_{[-1,1]}$, $K = 0.01$, with initial condition,

$$u(0,x) = 4\sin(x),$$
$$\rho(0,x) = \frac{1}{2\sqrt{\pi}}\left(e^{-\left(x+\frac{\pi}{2}\right)^2} + e^{-\left(x-\frac{\pi}{2}\right)^2}\right),$$

where $I_{[-1,1]}$ is the usual indicator function in $[-1, 1]$.

Our computation domain is $\Omega = [-2\pi, 2\pi] \times [-5, 5] \times [-1, 1]$, which is chosen to be large in order to include the range of $u, E, \rho$ at $t \approx 1$. The discretization parameters $\Delta x, \Delta p, \Delta q$ are chosen to be $0.04, 0.02, 0.02$ respectively, with $\tilde{\epsilon} = 0.009$, $\epsilon = 3\Delta x$ and CFL number 0.8.

In Fig. 6, multi-valued $u$ and $E$ are shown along with averaged density with peaks.

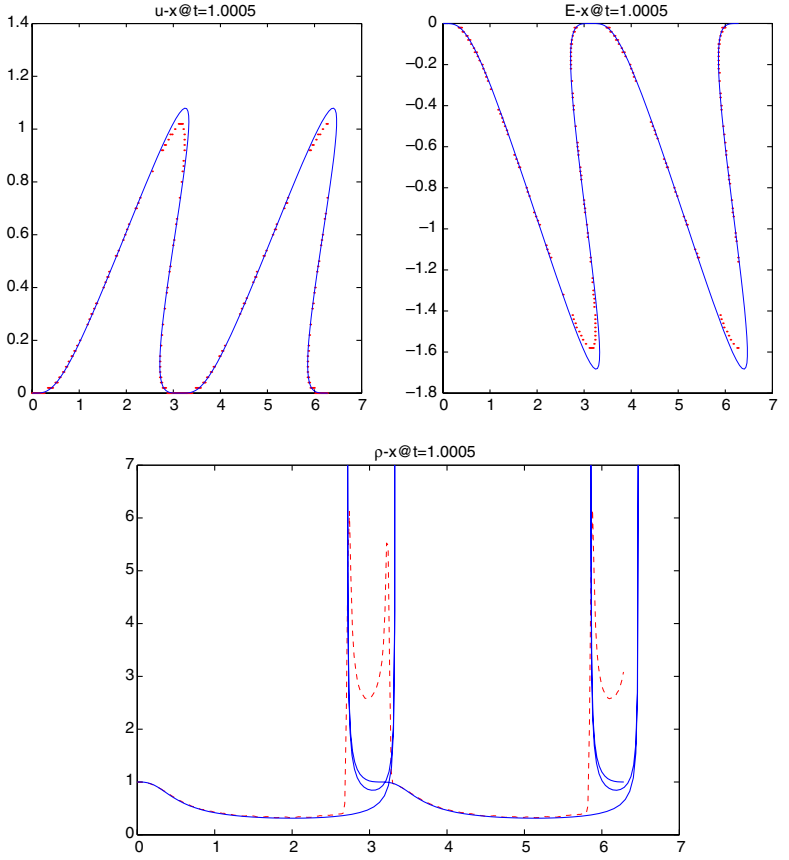


Fig. 5. Multi-valued solution for 1D Euler–Poisson equation at time around 1.

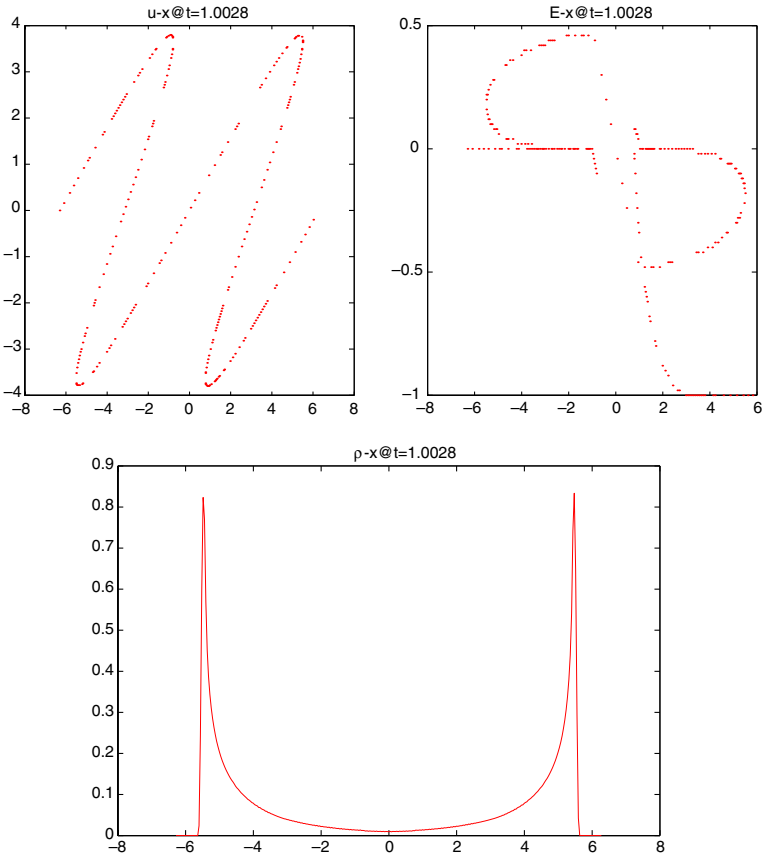


Fig. 6. Multi-valued solution for 1D Euler–Poisson equation at time around 1.

## 8. Conclusion

Together with [38] we have developed a field-space-based level set method for computing multi-valued solutions to 1D Euler–Poisson equations.

In field space multi-valued velocity and electric fields are naturally incorporated into the configuration, and represented implicitly by common zeros of two level set functions. Using those level set functions as building blocks, we further develop an implicit projection method to evaluate the multi-valued density as well as averaged velocity and electric fields. The main advantage of the proposed approach over phase-space-based method is its ability to unfold singularities in both velocity and electric fields. Moreover, the use of level set formulation enables us to easily treat any number of multi-valued branches, and the topology of multi-valued solutions is handled automatically.

Furthermore, we prove that the averaged density is simply a superposition of all multi-valued densities predicated by the characteristic method. Averaged field quantities are weighted superposition of corresponding multi-valued ones. This is remarkable since the underlying Euler–Poisson system is nonlinear!

The application of our method is not restricted to the computation of the semiclassical approximation of Schrödinger–Poisson equations. Similar problems arise in plasma oscillations, beam propagation, to which the techniques discussed in this paper is expected to be useful.

## Acknowledgments

The authors thank the anonymous referees who provide valuable comments resulting in improvements in this paper. This research was supported by the National Science Foundation under Grant DMS05-05975.

## References


[1] Y. Brenier, L. Corrias, A kinetic formulation for multi-branch entropy solutions of scalar conservation laws, Ann. Inst. Henri Poincare 15 (1998) 169–190.
[2] P. Burchard, L.-T. Cheng, B. Merriman, S. Osher, Motion of curves in three spatial dimensions using a level set approach, J. Comput. Phys. 170 (2001) 720–741.
[3] R.P. Beyer, R.J. LeVeque, Analysis of a one-dimensional model for the immersed boundary method, SIAM J. Numer. Anal. 29 (2) (1992) 332–364.
[4] R. Courant, D. Hilbert, Methods of Mathematical Physics. Vol. II: Partial Differential Equations (Vol. II by R. Courant.), Interscience Publishers (a division of John Wiley & Sons), New York–London, 1962, xxii+830, pp. 35.00.
[5] L.-T. Cheng, Efficient level set methods for constructing wave fronts in three dimensions, UCLA CAM report, 2006.
[6] L.-T. Cheng, H.-L. Liu, S. Osher, Computational high-frequency wave propagation in Schrödinger equations using the Level Set Method, with applications to the semi-classical limit of Schrödinger equations, Commun. Math. Sci. 1 (3) (2003) 593–621.
[7] M. Crandall, P.L. Lions, Viscosity solutions of Hamilton–Jacobi equations, Trans. AMS. Math. Soc. 277 (1) (1983) 1–42.
[8] L.-T. Cheng, S. Osher, M. Kang, H. Shim, Y.-H. Tsai, Geometry optics in a phase-space-based level set and Eulerian framework, J. Comput. Phys. 179 (2) (2002) 622–648.
[9] L.-T. Cheng, S. Osher, M. Kang, H. Shim, Y.-H. Tsai, Reflection in a level set framework for geometric optics, CMES Comput. Model. Eng. Sci. 5 (4) (2004) 347–360.
[10] B. Cockburn, J.L. Qian, F. Reitich, J. Wang, An accurate spectral/discontinuous finite-element formulation of a phase-space-based level set approach to geometrical optics. (English. English summary), J. Comput. Phys. 208 (1) (2005) 175–195.
[11] S. Engelberg, H.-L. Liu, E. Tadmor, Critical thresholds in Euler–Poisson equations (Dedicated to Professors Ciprian Foias and Roger Temam (Bloomington, IN, 2000)), Indiana Univ. Math. J. 50 (Special Issue) (2001) 109–157.
[12] B. Engquist, O. Runborg, Multi-phase computations in geometrical optics, J. Comp. Appl. Math. 74 (1996) 175–199.
[13] B. Engquist, O. Runborg, Computational high frequency wave propagation, Acta Numer. 12 (2003) 181–266 (Cambridge Univ. Press, Cambridge).
[14] B. Engquist, O. Runborg, T.-K. Tornberg, High frequency wave propagation by the segment projection method, J. Comput. Phys. 178 (2002) 373–390.
[15] B. Engquist, A.-K. Tornberg, R. Tsai, Discretization of Dirac delta functions in level set methods, J. Comput. Phys. 207 (1) (2005) 28–51.
[16] M.-G. Forest, H. Flaschka, D.-W. Mclaughlin, Multi-phase averaging and the inverse spectral solution of the Korteweg–de Vries equation, Comm. Pure Appl. Math. 33 (1980) 739–784.
[17] S. Fomel, J.A. Sethian, Fast-phase space computation of multiple arrivals, Proc. Natl. Acad. Sci. 99 (11) (2002) 7329–7334.
[18] I. Gasser, D. Levermore, P. Markowich, C. Schmeiser, The initial time layer problem and the quasineutral limit in the semiconductor drift-diffusion model, European J. Appl. Math. 12 (4) (2001) 497–512.
[19] P. Gerard, P.A. Markowich, N.J. Mauser, F. Poupaud, Homogenization limits and Wigner transforms, Comm. Pure Appl. Math. 50 (1997) 323–380.
[20] L. Gosse, Using K-branch entropy solutions for multivalued geometric optics computations, J. Comput. Phys. 180 (2002) 155–182.
[21] L. Gosse, S. Jin, X. Li, On two moment systems for computing multiphase semiclassical limits of the Schrödinger equation, Math. Models Methods Appl. Sci. 13 (12) (2003) 1689–1723.
[22] L. Gosse, P.A. Markowich, Multiphase semiclassical approximation of an electron in a one-dimensional crystalline lattice. I. Homogeneous problems, J. Comput. Phys. 197 (2) (2004) 387–417.
[23] L. Gosse, N.J. Mauser, Multiphase semiclassical approximation of an electron in a one-dimensional crystalline lattice —III. From ab initio models to WKB for Schrödinger–Poisson, J. Comput. Phys. 211 (2006) 326–346.
[24] Y. Guo, Smooth irrotational flows in the large to the Euler–Poisson system in $\mathbf{R}^{3+1}$, Comm. Math. Phys. 195 (2) (1998) 249–265, Reviewer: Woodford W. Zachary.
[25] R. Hutter, Beam and Wave Electronics in Microwave Tubes, D. Van Nostrand Company, Inc., Princeton, 1960.
[26] S. Jin, X. Li, Multi-phase computations of the semiclassical limit of the Schrödinger equation and related problems: Whitham vs Wigner, Physica D 182 (2003) 46–85.
[27] S. Jin, H.-L. Liu, S. Osher, Y.h. Tsai, Computing multivalued physical observables for the semiclassical limit of the Schrö dinger equation, J. Comput. Phys. 205 (1) (2005) 222–241.
[28] S. Jin, H.-L. Liu, S. Osher, Y.H. Tsai, Computing multi-valued physical observables for the high frequency limit of symmetric hyperbolic systems, J. Comput. Phys. 210 (2005) 497–518.
[29] S. Jin, S. Osher, A level set method for the computation of multivalued solutions to quasi-linear hyperbolic PDE's and Hamilton–Jacobi equations, Comm. Math. Sci. 1 (3) (2003) 575–591.
[30] H.-L. Liu, L.-T. Cheng, S. Osher, A level set framework for capturing multi-valued solutions to nonlinear first-order equations, J. Sci. Comp. (2005) (December 07 (electronically)).
[31] P. Lax, D. Levermore, The small dispersion limit of the Korteweg–de Vries equation. I., Comm. Pure Appl. Math. 36 (3) (1983) 253–290.
[32] P. Lax, D. Levermore, The small dispersion limit of the Korteweg–de Vries equation. II., Comm. Pure Appl. Math. 36 (5) (1983) 571–593.
[33] P. Lax, D. Levermore, The small dispersion limit of the Korteweg–de Vries equation. III., Comm. Pure Appl. Math. 36 (6) (1983) 809–829.

[34] H.-L. Liu, S. Osher, Y.H. Tsai, Multi-valued solution and level set methods in computational high frequency wave propagation, Commun. Comput. Phys. 1 (5) (2006) 765–804.
[35] P.-L. Lions, T. Paul, Sur les measures de Wigner, Revista. Mat. Iberoamericana 9 (1993) 553–618.
[36] S.Y. Leung, J.L. Qian, S. Osher, A level set method for three-dimensional paraxial geometrical optics with multiple point sources, Commun. Math. Sci. 2 (4) (2004) 643–672.
[37] H.-L. Liu, E. Tadmor, Semi-classical limit of the nonlinear Schrödinger–Poisson equation with subcritical initial data, Methods Appl. Anal. 9 (4) (2002) 517–532.
[38] H.-L. Liu, Z.-M. Wang, Computing multi-valued velocity and electrical fields for 1d Euler–Poisson equations, Appl. Numer. Math., in press.
[39] X. Li, J. Wöhlbier, S. Jin, J. Booske, An Eulerian method for computing multi-valued solutions of the Euler–Poisson equations and applications to wave breaking in klystrons, Phys. Rev. E 70 (2004) 016502.
[40] P. Markowich, N. Mauser, The classical limit of a self-consistent quantum-Vlasov equation in 3-D, Math. Models Methods Appl. Sci. 3 (1) (1993) 109.12.
[41] P. Markowich, C. Ringhofer, C. Schmeiser, Semiconductor Equations, Springer, Vienna, 1990.
[42] S. Osher, L.-T. Cheng, M. Kang, H. Shim, Y.-H. Tsai, Geometric optics in a phase space based level set and Eulerian framework, J. Comput. Phys. 179 (2002) 622–648.
[43] J. Qian, L.-T. Cheng, S. Osher, A level set based Eulerian approach for anisotropic wave propagation, Wave Motion 37 (2003) 365–379.
[44] P.-A. Raviart, An analysis of particle methods, in: Numerical Methods in Fluid Dynamics (Como, 1983), Lecture Notes in Math., vol. 1127, Springer, Berlin, 1983, pp. 243–324.
[45] Leonid Ryzhik, George Papanicolaou, Joseph B. Keller, Transport equations for elastic and other waves in random media, Wave Motion 24 (4) (1996) 327–370.
[46] O. Runborg, Some new results in multi-phase geometric optics, Math. Model. Numer. Anal. 34 (2000) 1203–1231.
[47] C.-W. Shu, High order ENO and WENO schemes for computational fluid dynamics, High-order Methods for Computational Physics, Lect. Notes Comput. Sci. Eng., vol. 9, Springer, Berlin, 1999.
[48] C. Sparber, P.A. Markowich, N.J. Mauser, Wigner functions versus WKB-methods in multivalued geometrical optics, Asymptot. Anal. 33 (2) (2003) 153–187.
[49] W. Symes, J. Qian, A slowness matching Eulerian method for multivalued solutions of Eikonal equations (Special issue in honor of the sixtieth birthday of Stanley Osher), J. Sci. Comput. 19 (1–3) (2003) 501–526.
[50] A.-K. Tornberg, B. Engquist, Regularization techniques for numerical approximation of PDEs with singularities Special issue in honor of the sixtieth birthday of Stanley Osher, J. Sci. Comput. 19 (1–3) (2003) 527–552.
[51] A.-K. Tornberg, B. Engquist, Numerical approximations of singular source terms in differential equations, J. Comput. Phys. 200 (2) (2004) 462–488.
[52] Y.-H.R. Tsai, Y. Giga, S. Osher, A level set approach for computing discontinuous solutions of Hamilton–Jacobi equations, Math. Comp. 72 (2003) 159–181.
[53] J. van Trier, W.W. Symes, Upwind finite-difference calculation of traveltimes, Geophysics 56 (1991) 812–821.
[54] E. Wigner, On the quantum correction for thermodynamic equilibrium, Phys. Rev. 40 (1932) 749–759.
[55] G. Whitham, Linear and Nonlinear Waves, Wiley, New York, 1974.
[56] P. Zhang, Y.X. Zheng, N. Mauser, The limit from the Schröinger-Poisson to the Vlasov–Poisson equations with general data in one dimension, Comm. Pure Appl. Math. 55 (5) (2002) 582–632.